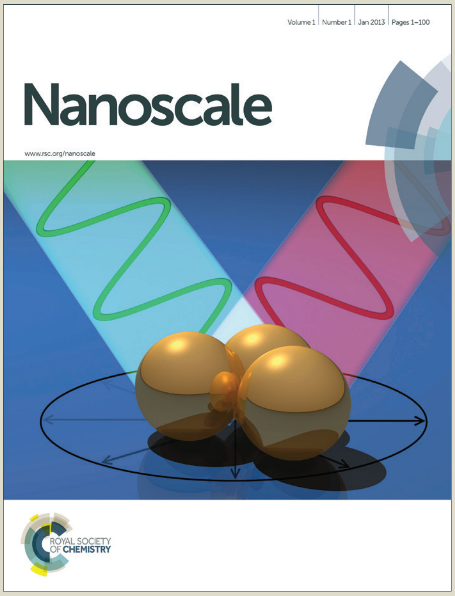
Volume 1 | Number 1 | Jan 2013 | Pages 1–100
Nanoscale
www.rsc.org/nanoscale
ROYAL SOCIETY OF CHEMISTRY

Nanoscale RSCPublishing

ARTICLE

Predictable and Controllable Dual-phase Interfaces in TiO_2 (B)/Anatase Nanofibers

Cite this: DOI: 10.1039/x0xx00000x

Yimin Lei, [a, b, c] Jie Sun, [a, b, c] Hongwei Liu, [c] Xuan Cheng, [d] Fuyi Chen, [b, *] and Zongwen Liu [a, *]

Received 00th January 2012,
Accepted 00th January 2012

DOI: 10.1039/x0xx00000x

www.rsc.org/

The TiO_2 (B)/anatase dual-phase nanofiber exhibits enhanced photocatalytic activity when interfaces form during phase transformation of TiO_2. To precisely control the formation of coherent interfaces between TiO_2 (B) and anatase, a thorough knowledge of phase transformation particularly from TiO_2 (B) to anatase (TA) is required. In our study, a crystallography model in conjunction was employed to investigate the phase transformation. The coherent interface with a crystallographic orientation relationship of $[001]_{TB}//[100]_{TA}$, $(200)_{TB}//(002)_{TA}$, and $(020)_{TB}//(020)_{TA}$ predicted by the crystallography model were also observed by TEM experimentally. In addition, two types of incoherent interfaces that may deteriorate photocatalytic activity were examined and can be eliminated via an accurate tuning of calcination. The fundamental knowledge acquired from this work, therefore, provide new insight to synthesis more efficient dual-phase TiO_2 photocatalysts.

Introduction

TiO_2 is an important functional oxide with unique photoelectrochemial properties. It has growing applications in solar cells,[1] lithium batteries,[2, 3] and photocatalyst[4-6] et al. There are mainly four types of TiO_2 polymorphs. They are anatase, rutile, brookite and TiO_2 (B), respectively.[7] In photocatalysts, mixed-phase TiO_2 nanostructures are shown to be more efficient than single TiO_2 polymorph.[8] Anatase/rutile mixed-phase nanoparticles (Degussa P25[9]) is a well-known example. Because of a band alignment of ~ 0.4 eV between anatase and rutile,[10] the anatase/rutile mixed-phase interfaces can significantly enhance the working efficiency of TiO_2 photocatalyst.[4, 11] Although such interfaces can be obtained by mechanically mixing anatase and rutile, it is difficult to acquire real dual-phase anatase/rutile interfaces. The fact is due to the difficulty in controlling the martensitic phase transition from anatase to rutile.[12] However, this is a different case for TiO_2(B)/anatase system. As the TiO_2 (B)-anatase transformation is a typical diffusional phase transition, photocatalysts with high efficiency can be produced by achieve dual-phase interfaces between TiO_2 (B) and anatase via phase transformation. The previous work demonstrates that the excellent spatial charge separation from the dual-phase TiO_2(B)/anatase interfaces[6, 13, 14] leads to enhanced photocatalytic activity, stability and easy-recovery properties in TiO_2(B)/anatase core-shell nanofibers.[6, 15-18] Moreover, the efficiency of TiO_2 photocatalysts can be further promoted if the dual-phase interfaces is coherent instead of being incoherent. This is because the electrons or holes can pass through the coherent interfaces easier than through the incoherent interfaces. Therefore, the design and control of the dual-phase interfaces are of significant, in order to enhance the properties of the TiO_2 photocatalysts.

Calcinating TiO_2 (B) nanostructures directly[15] is a feasible and low-cost way to obtain dual-phase TiO_2(B)/anatase interfaces, owing to the phase transformation from TiO_2 (B) to anatase. By controlling the transformation process, different interfaces with different crystallographic orientation relationships (CORs) can be achieved. The diversity of interface structures induced by different CORs will strongly affect the charge transfer properties. Therefore, the control of phase transition is one of the most effective way to design and obtain the wanted dual-phase interfaces with enhanced catalytic performance in TiO_2 photocatalysts.

In the past, the TiO_2 (B)/anatase phase transformation has been investigated mainly in bulk system. Brohan[19] has explained the transformation by the shear of $\mathbf{(\bar{2}01)_{TB}}$ plane to form $\mathbf{(10\bar{3})_{TA}}$ plane (Here, “TA” and “TB” represents anatase and TiO_2 (B), respectively), along the $\mathbf{[\bar{2}0\bar{3}]_{TB}}$ direction. In 1991, Banfield[20] has showed that TiO_2 (B) polymorph could be converted to anatase either via the growth of the two structures, or via a bulk mechanism when anatase nuclei were scarce or absent. However, the detailed phase transformation has not been discovered in nanoscaled system so far. In terms of the related interfaces, aside from a few studies,[6, 18] there is limited thorough investigation, especially in the detailed characterization of crystallographic features, the precise calculation and prediction on crystallography. Liu et al[21] have used the invariant line strain theory model to calculate the coherent interfaces within TiO_2 nanofibers. However, the calculation is too complicated to use, and consequently provides limited contribution to the design of new and improved dual-phase TiO_2 photocatalysts.

In this work, the phase transformation and resulted dual-phase interfaces in TiO_2 (B)/anatase system are investigated experimentally and theoretically. The experimental results from transmission electron microscopy (TEM) and the prediction of phase transformation and dual-phase interfaces calculated by crystallography model are consistent with each other. The present study will not only help better understand the interface-controlled catalytic effect but also prompt the design of a new class of catalysts with improved performance.

Experimental Section

The $H_2Ti_3O_7$ nanofibers (The detailed synthesis process can be found in previous work[22]) were calcinated at 650 °C (S-650, for 2 hours) and 700 °C (S-700, for 2 hours) in air respectively. Then the obtained products, S-650 and S-700 were dispersed onto copper grids with carbon film. A JEOL 2200FS TEM (200KV) was used to characterize the nanofibers. Meanwhile, invariant deformation element (IDE) crystallography model for diffusional phase transformation[23] was applied to predict dual-phase interfaces observed during the phase transition from TiO_2 (B) to anatase in the nanofibers. The calculated results were compared with the experimental outcomes.

Results

In Fig. 1, the bright field (BF), dark field (DF), selected area electron diffraction (SAED) and high-resolution transmission electron microscopy (HRTEM) were performed on a S-650 nanofiber with a length of 3 μm and an aspect ratio of 0.033. According to the SAED pattern (Fig.1 (d)), TiO_2(B) (TB) and anatase (TA) coexist in the fiber, and their crystallographic orientation relationship (COR) can be expressed as $[001]_{TB}//[100]_{TA}$, $(200)_{TB}//(002)_{TA}$ and $(020)_{TB}//(020)_{TA}$, denoted as COR-I. In order to distinguish the two phases, DF image (Fig. 1(c)) from the yellow rectangle area in Fig. 1(a) was acquired through the diffraction spot (620) $_{TB}$. It is well matched with the BF image in Fig. 1(b). Additionally, the interface can also be clearly observed from the HRTEM image in Fig. 1(e).

In order to better understand the dual-phase interface and detailed COR between the TB and TA phases, the HRTEM image was analysed with fast Fourier transform (FFT) and inverse fast Fourier transform (IFFT) as shown in Fig. 2(a)-2(c). According to Fig. 2(a-b), the interface between the TB and TA is coherent. The FFT demonstrates that the orientations of the two phases at each sides of interface are $[001]_{TB}$ and $[100]_{TA}$ respectively. Meanwhile, the relationships of $(200)_{TB}//(002)_{TA}$ and $(020)_{TB}//(020)_{TA}$ also can be seen. The FFT result is consistent with SAED pattern in Fig. 1(d). Both of them indicate the connections between $(200)_{TB}$ and $(002)_{TA}$, and $(020)_{TB}$ and $(020)_{TA}$ at the interface area, which show agreement with previous report[6], in which the Fig. 5(d) displayed the detailed connection between the two phases.

In fact, the formation of the coherent dual-phase interface is attributed to the coherent match between the two phases along orientations of $[001]_{TB}$ and $[100]_{TA}$respectively, indicating the interfaces can be obtained with the preferred COR between two related phases. Thus, the controlling of dual-phase interfaces can be further simplified to the control of phase transition from TB to TA. In this case, with the deep understanding of the detailed process of such phase transition, it is possible to manipulate the dual-phase interfaces through ways of controlling the temperature, calcinating speed, doping or adding specific chemicals et al.

In the present work, the TB/TA nanosystem is theoretically predicted by the IDE model, a useful and practical model to predict phase transformation process, which has shown reliable results in the past.[23, 24] In this work, even though the phase transition is involved with nanosystem, it can still be predicted.[21] The space group of the initial phase TB and newly formed phase TA are C2/m and I41/amd, respectively. The transition between them is a typical monoclinic-to-tetragonal process. The lattice correspondence along 3 directions for this transition which are can be drawn in the stereographic projection of planes, as shown in Fig. 2f. $(1\bar{1}0)^*{}_{TB}//(0\bar{1}1)^*{}_{TA}$, $[110]_{TB}//[111]_{TA}$ and $[2,2,13]_{TB}//[\bar{7}11]_{TA}$,[25] the main strain along the three lattice correspondence directions are denoted as η_1, η_2 and η_3 respectively.

Therefore, on the coordinate system of TB lattice, the Bain strain matrix can be expressed as equation (1). Regarding the selection of lattice correspondence between the two phases, it is discussed in detail later.

$$\boldsymbol{B}=\begin{pmatrix}\eta_1 & 0 & 0\\ 0 & \eta_2 & 0\\ 0 & 0 & \eta_3\end{pmatrix}=\begin{pmatrix}\frac{|3[7\bar{1}\bar{1}]_{TA}|}{|[2,2,13]_{TB}|} & 0 & 0\\ 0 & \frac{|(011)^*_{TA}|}{|(1\bar{1}0)^*_{TB}|} & 0\\ 0 & 0 & \frac{|[111]_{TA}|}{|[110]_{TB}|}\end{pmatrix} \tag{1}$$

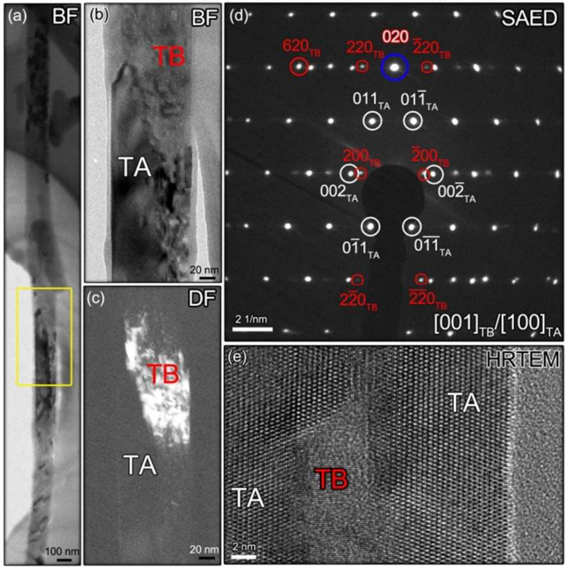

Figure 1 TEM characterization on a dual-phase TB/TA nanofiber. (a) the BF image of whole fiber; center BF image (b) and center DF image using $(620)_{TB}$ diffraction spot (c) from yellow rectangle area in panel (a); (d) SAED pattern of nanofiber; (e) HRTEM image from one dual-phase area.

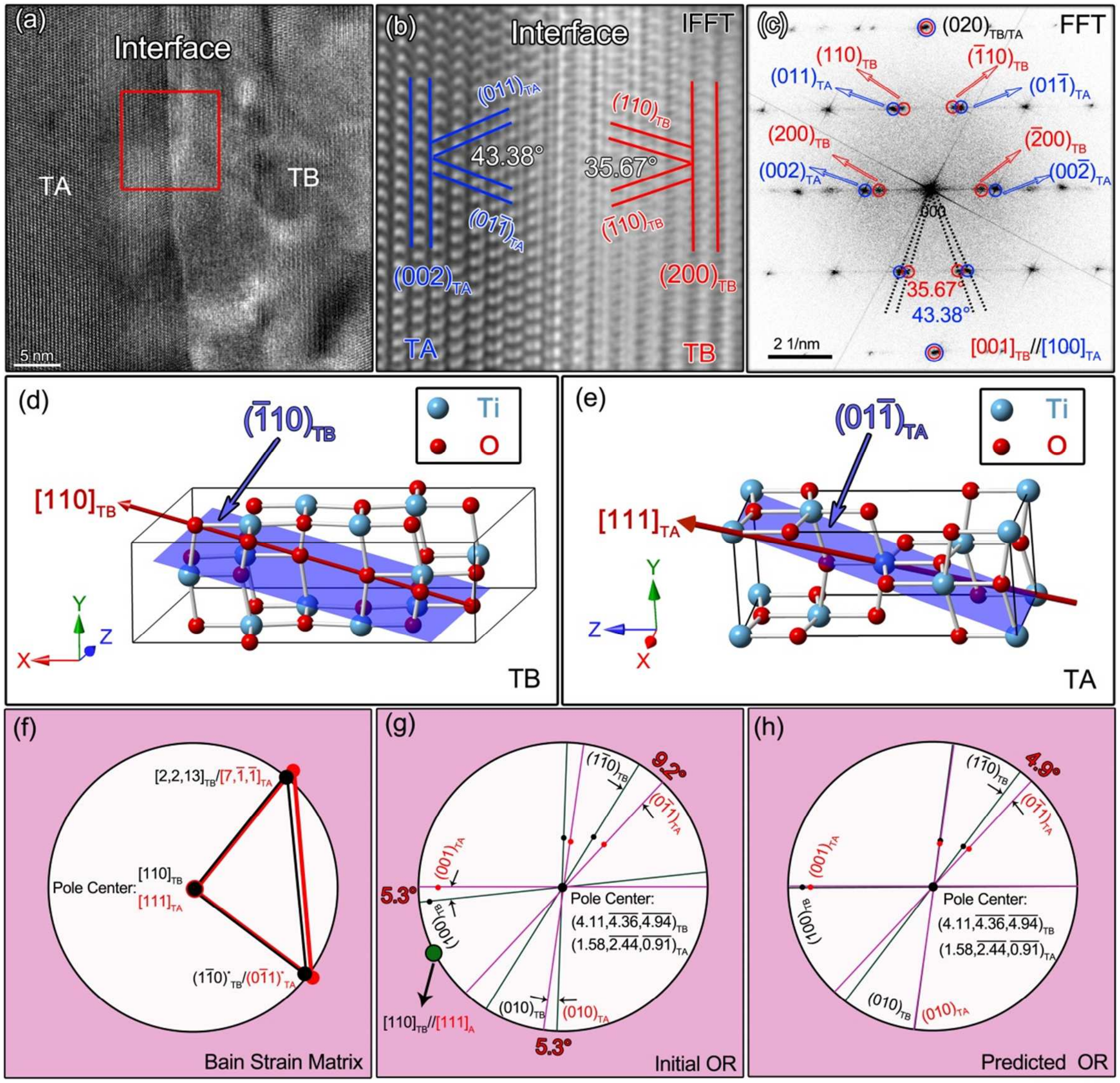

Figure 2 (a) High resolution transmission electron microscope (HRTEM) image of dual-phase area in nanofiber coexisting phases of TB and TA; (b) Inverse fast Fourier transform (IFFT) image of corresponding to panel a; (c) Fast Fourier transform (FFT) image and the index of crystallographic orientation relationship of TB/TA reaction system in panel a; The schematic of TB (d) and TA (e) crystal structure; (f) The lattice rearrangement and corresponding relationship of TB/TA system; The orientation relationship of TB/TA system before rotation (g) and after prediction (h).

In monoclinic structure, the [010] vector is commonly chosen as the Burgers vector, because it is the shortest vector in the Bravais lattice.[26] In the real crystal structure of TB, however, the vector $[032]_{TB}$ in the close-packed plane is actually shorter than $[010]_{TB}$. Therefore, $[032]_{TB}$ is selected as the Burgers vector instead of $[010]_{TB}$. The detailed calculation process can be found in the supplementary materials. The comparison between the predicted and experimental results for the TB/TA system is listed in Table 1.

To compare to the TEM results (Fig. 2a-c), the initial and predicted CORs were represented with stereographic projection of planes. The pole centers used in Fig.2(g) and (h) are normal planes corresponding to the $[001]_{TA}$ and $[100]_{TB}$ directions with the index of $(4.11,\overline{4.36},\overline{4.94})_{TB}$ and $(1.58,\overline{2.44},\overline{0.91})_{TA}$ in respective coordinate systems. The green spot in Fig. 2(g) indicates that the mutual relationship between TB and TA is consistent with the Bain strain matrix. There is mutual rotation of 5.3° from the initial COR to the final COR. The result demonstrates the final COR displayed in the TEM results can be obtained through one-step rotation from initial corresponding relationship expressed by Bain strain matrix. The rotation angle calculated by the model is 4.3° (shown in the table 1 in supporting information). Therefore, the predicted result agrees well with TEM result with a small discrepancy of 1°. In addition, the habit plane (HP) and growth direction (GD) were also obtained by the IDE model, as shown in Table 1. The predicted HP is consistent with experimental HP with discrepancy of 1.6°. As for the GD, it is expected to be proved in future work.

Table 1 The comparison between the experimental and predicted results.

	Experimental Results	Predicted Results	δ

OR	$[001]_{TB}//[100]_{TA}$
	$(200)_{TB}//(002)_{TA}$
	$(020)_{TB}//(020)_{TA}$
		$[001]_{TB}//[100]_{TA}$
		$(200)_{TB} \overset{1^\circ}{\Rightarrow} (002)_{TA}$
		$(020)_{TB} \overset{1^\circ}{\Rightarrow} (020)_{TA}$
			1°

(Habit Plane)*	$[905]_{TB}$	$[8\bar{1}5]_{TB}$	1.6°
Habit Plane	$(100)_{TB}$	$(10.733, 0.141, 0.231)_{TB}$	1.6°
Growth Direction	NA	$[2,13,1]_{TB}$	NA

Remarks: The detailed calculation process can be found in the support information. The asterisk "*" used in table expresses the planar normal.

In summary here, the IDE calculated results indicate that the phase transformation system of TB/TA with nanoscale size can be precisely predicted by the crystallography model. The detailed information of interfaces in such titania nanocomposites thus can be predicted through IDE without difficult experiments. Moreover, other crystallography features, such as HP and GD et al can also be predicted. Lack of GD measurement in present work is due to the fabricated morphology and the limitation of the rotating geometry system of TEM instrument. It is proposed such GD can be observed in bulk TB material.

Aside from the above finding, two other incoherent dual-phase interfaces with COR-II (Fig. 3(a-d)) and COR-III (Fig. 3(e-h)) have been identified in the S-700 nanofibers, as presented in Fig. 3. Based on corresponding FFT images, the COR-II can be expressed as $[001]_{TB}//[011]_{TA}$ and $(200)_{TB}//(011)_{TA}$, and the COR-III can be displayed as $[1\bar{7}6]_{TB}//[100]_{TA}$ and $(\bar{6}01)_{TB}//(022)_{TA}$. Here, the steps are clear in both of the two interfaces, which are the feature of incoherent interface. Thus, interfaces with the three kinds of COR (I, II and III) are different from each other. The fact is further supported by the evidence that the FFT images of COR-II and COR-III have different zone axes $[011]_{TA}$ and $[1\bar{7}6]_{TB}$ parallel to the orientations of $[001]_{TB}$ and $[100]_{TA}$ respectively which implies the COR-II and COR-III interfaces are different from the COR-I interface. Further works will be required to verify the detailed structures of COR-II and COR-III interfaces.

Discussion

1 How to achieve the prediction?

In this work, to achieve the prediction on the coherent dual-phase interfaces, choosing appropriate lattice correspondence and Burgers vector is the key. The choosing process is simple and easily understanding.

First of all, it is necessary to explain why the η_1, η_2 and η_3 were chosen as the lattice correspondence. When the crystal structure includes face-centred or body-centred atoms, the directions parallel to the diagonal line or body diagonal line deserve much attention, because the face-centred and body-centred atoms are critical atoms in phases with complex cell structures, and they strongly influence the phase transformation.

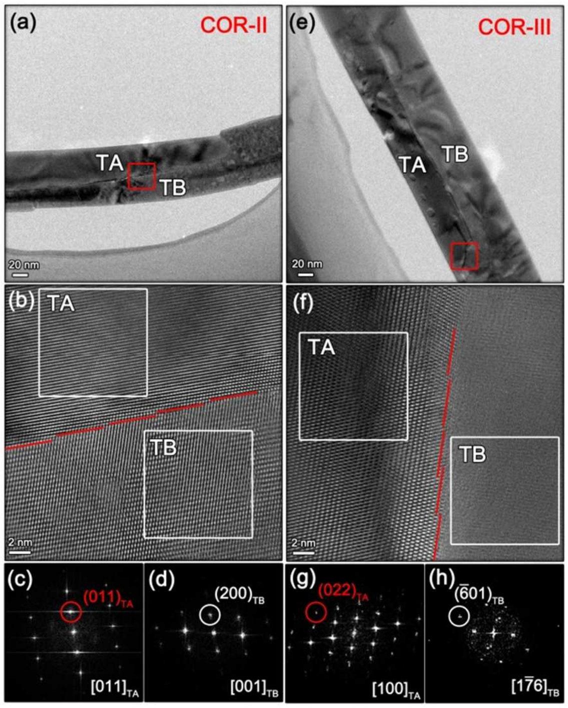

Figure 3 BF, HRTEM and corresponding FFT images of the nanofibers heated at 700 °C for 2 hours in air, which indicates the dual-phase TB/TA interfaces with (a-c) COR-II and (d-f) COR-III.

According to the space groups of the TB/TA reaction system, it is reasonable to choose the face diagonal line of $[110]_{TB}$ (Fig. 2(d)) in the initial phase TB (the C-centred crystal) parallel to the body diagonal line of $[111]_{TA}$ (Fig. 2(e)) in phase TA (the body-centred crystal). Therefore, the η_3 was chosen as $[110]_{TB}//[111]_{TA}$ accordingly.

In terms of η_2, there are two aspects to be considered. The $\{110\}_{TB}$ and $\{011\}_{TA}$ are closed-packed facets in TB and TA structures respectively, which always play a key role during phase transformation.[27] In addition, on the basis of the experimental result, the diffraction spots of the $\{110\}_{TB}$ planes are barely seen in the SAED pattern shown in Fig. 1(d), whereas the diffraction spots of $\{011\}_{TA}$ is significantly intensive. The weakening of diffraction patterns of $\{110\}_{TB}$ planes indicates that $\{110\}_{TB}$ planes have already transformed to be planes of $\{011\}_{TA}$. Therefore, the normal directions of $(1\bar{1}0)_{TB}$ and $(011)_{TA}$,which belong to $\{110\}_{TB}$ and $\{011\}_{TA}$ respectively are selected as another main strain directions. They are $[2,\overline{19},1]_{TB}$ and $[0,19,\bar{3}]_{TA}$ respectively. Moreover, the angles of $[110]_{TB} - [2,\overline{19},1]_{TB}$ and $[111]_{TA} - [0,19,\bar{3}]_{TA}$ are very close to 90°. Then, η_2 was settled in this way. In addition, η_1 has been also identified based on the reference coordinate system and stereographic projections.[25]

In terms of the selection of Burgers vectors, in general, the selection of Burgers vector is relatively easy for simple crystal structures for phase transition calculation. For example, in the case of cubic-to-cubic phase transition,[28] only 1/2 <110> can be chosen as the Burgers vector for calculation. For complex monoclinic-to-tetragonal system, however, the selection of Burgers vector not only depends on Bravais lattice, but also on the real crystal structure. As aforementioned, in the real lattice of TB, $[032]_{TB}$ vector is shorter than [010]vector, the shortest vector in common monoclinic Bravais lattice. It consequently was chosen as Burgers vector in this case.

Actually, the invariant line strain (ILS) theory[29] is another method that has been previously used to study the crystallographic features of TB/TA reaction system.[21] Both IDE and ILS are found to have equal level of discrepancy. However, the IDE model is much easier to understand and simpler to be applied than the ILS theory because of only one-step rotation needed in the calculation. Thus, it is a better approach to study the TB/TA system as well as other complex phase transformations in nanosystem.

2 The applicability of the prediction method

Here, someone may argue that the successful prediction of the coherent interfaces in the TiO_2 (B)/anatase dual-phase nanofiber might be just one specific case. The fact is that the method has already predicted the monoclinic-to-monoclinic nanosystem in our previous work, in which the experimental results show precise agreement with the predicted results for the $H_2Ti_3O_7/TiO_2$ (B) system, although it is a relatively simply system compared to the monoclinic-to-tetragonal system.[27] As for the case in anatase/rutile nanosystem, the famous martensitic phase transition system, it is expected the experimental results is consistent with the already obtained the predicted results in future.

3 Atomic Mechanism of phase transition from TB to TA

Based on the, predicted results, TEM experiments and fundamental building blocks (FBB) model[30], the interpretation of phase transition from TB to TA is shown in Fig. 4.

In Fig. 4(a), the view direction are $[001]_{TB}$ and $[100]_{TA}$ for TB and TA phases respectively, which also are the zone axes in TEM results in Fig. 1-2. The angle has significant expanding from 35.67° (angle between $(110)_{TB}$ and $(\bar{1}10)_{TB}$) to 43.38° (angle between $(011)_{TA}$ and $(01\bar{1})_{TA}$) within the octahedral layer, which is consistent with SAED result (Fig. 1(d)) that the $\{110\}_{TB}$ diffraction patterns were substituted by those of $\{011\}_{TA}$. Additionally, the slippage of half TiO_6 octahedral between the octahedral layers of TB phase is eliminated after phase transformation. Such change is strongly related to the angel expanding observed, which eventually results in the shrinkage from the initial cell parameter *a* of TB (1.2208 nm) to the cell parameter *c* of TA (0.9515 nm).

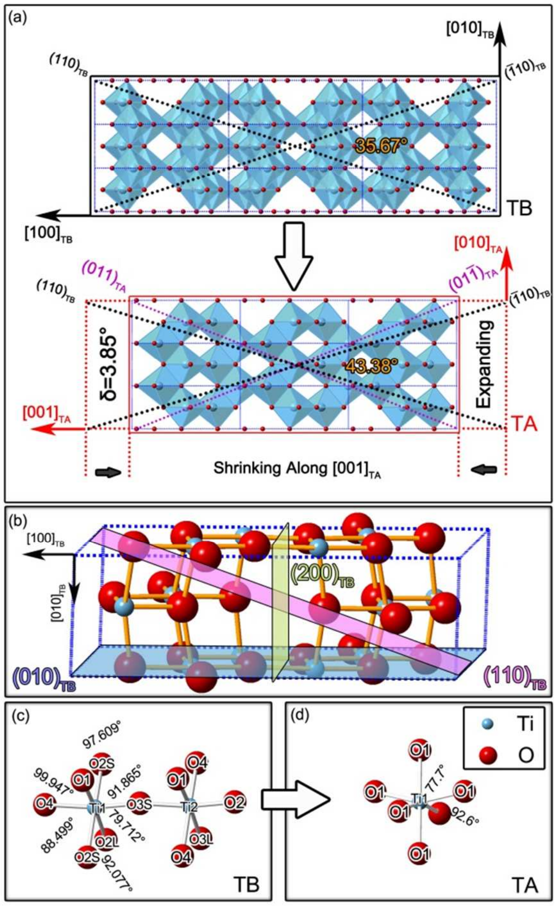

Figure 4 The interpretation of phase transformation from TB to TA: (a) angle expanding explanation by FBB model; (b) the important planes in TB unit cell; Bond angles in TB (c) and TA (d) crystal structures.

It is known that the phases of TB and TA contain 24 atoms and 12 atoms per unit cell, respectively. Each Ti atom is coordinated to six O atoms and each O atom is coordinated to three Ti atoms for both TB and TA phases. In each phase, the TiO_6 octahedron is slightly distorted, with all of the O-Ti-O bond angles deviating from 90°. Such distortion is greater in TB (Fig. 4(c)) than in TA (Fig. 4(d)). The essential difference is that there are 10 different Ti-O bonds, ranging from 1.813 to 2.255 Å in TB.[31] In contrast, there are only two types of Ti-O bonds and O-Ti-O bond angels in TA.[32] TB has a more complicated structure than TA. According to Fig. 4(b), the $(110)_{TB}$ plane cuts through 8 Ti-O bonds. The $(200)_{TB}$ plane cuts through 4 Ti-O bonds, while the $(010)_{TB}$ does not cut through any bonds. Therefore, the $(110)_{TB}$ plane is most active plane compared to the other two planes. The angle expanding involved $\{110\}_{TB}$ planes thus results in significant changes within and between the TiO_6 octahedron layers. In addition, the SAED result (Fig. 1(d)) indicates that the following changed plane is $(200)_{TB}$. The fact is consistent with the proof that $(200)_{TB}$ is the second higher active plane. Similarly, the $(010)_{TB}$ plane which keep away from any Ti-O bonds leads to the invariant of diffraction spots during the transformation.

The angle expanding displayed in Fig. 4(a) can also be illustrated by the change of O-Ti-O bond angles. During calcination process, the more distorted TB structure transforms to TA structure with higher symmetry when the TB atoms obtain enough energy. Clearly, the 6 different O-Ti-O bond angles from TB change to be TA with only 2 smaller and more stable O-Ti-O bond angles. Since the energy of system show inversely proportional relationship with bond angle, it is believed that the transformation from TB to TA is a reasonable process from the perspective of energy.

4 Multi-incoherent dual-phase TB/TA interfaces

The coherent dual-phase interface with COR-I has been discovered not only in present work, but also in previous study.[16, 21] It is a typical TB/TA interface in such system. Coherent interface with COR of $[100]_{TB}//[001]_{TA}$ has also been reported previously[18]. Aside from the two coherent interfaces, another major finding in the this work is the discovery of two incoherent dual-phase TB/TA interfaces, as shown in Fig. 3. The fact implies that TB/TA nanosystem has huge potential to discover variety of dual-phase interfaces to serve as the photocatalysts. Moreover, these interfaces can be predictable and further controlled from calculated results.

In addition, the two incoherent interfaces in Fig. 3(b) and (f) both show steps. However, the $(200)_{TB}$ plane, which is equivalent to $(100)_{TB}$ plane, the HP in the phase transformation with coherent interface with COR-I, as shown in Fig. 2(b), is ordered and without any step. Generally speaking, the HP observed experimentally, was clean and with the smallest surface mismatch and fewest steps.[29] The comparison of the steps between the coherent and incoherent interfaces indicates that competition must exist between the these CORs, which could be explained by the features of the respective matching planes in TB and TA phases. Owing to involving the orientation with minimum indexing, the phase transition with COR-I of $[001]_{TB}//[100]_{TA}$ is the easier way to take place phase transformation than the other two.

5 Designable dual-phase interfaces

In present work, three types of CORs between TB and TA were observed, corresponding to three different dual-phase interfaces. The interface with COR-I is flat and fully coherent with high elastic strain, while the other two are incoherent with variety of steps. The interfaces are related to crystal structure and chemical potential.

Regarding the crystal structure, coherent interface exhibit higher density of coincident sites for both phases and thus much more stable with lower interface energy than incoherent interfaces. In the respect of chemical potential, chemical bonds distributed at coherent interface contact tightly with each other, and relatively low chemical potential is acquired to generate bonds.[21, 33] In this work, the COR-I interface, as a typical coherent interface is more stable and favourite compared to the other two. It is believed that electrons and holes can pass through easily from coherent interfaces with less broken bond and misfits. , such interfaces consequently show enhanced photocatalytic activity.[34]

Furthermore, COR-II and COR-III interfaces were obtained at higher temperature (S-700), whereas the condition of 600 °C and 2 hours is already suitable for COR-I interface, indicating that the interfaces are sensitive to the reaction temperature and calcinating time. Therefore, by precisely controlling the phase-transformation condition, coherent interfaces with COR-I could be obtained and retained, while the probability of the other two can be eliminated. Accordingly, we can design such new-composite of titania with favourite interfaces to perform better photocatalytic property.

Moreover, not only for the titania photocatalysts (also including the system of anatase/rutile), but also for other areas, such as transistor, lasers, and solar cell which all already exploit interfacial phenomena,[35] the knowledge acquired in present work could shed on the research on the areas in terms of prediction of interfaces.

Conclusions

In summary, TEM results show there are three types of dual-phase interfaces with three different CORs in the TB/TA nanosystem. IDE model is applied as a simple and practical crystallography model to calculate the crystallographic information on the coherent dual-phase TB/TA interface. The consistency of the theoretical calculation and the TEM results indicates that a feasible way to design and further control the interfaces in dual-phase titania photocatalysts by IDE model is available. In addition, the mechanism of phase transition from TB to TA is successfully interpreted. The angle expanding is believed to be the driving force to such phase transformation. On the other hand, the multiple interfaces with different CORs are also discussed via competition mechanism, which indicates the interface with COR-I of $[001]_{TB}//[100]_{TA}$ is a typical coherent interface in TB/TA nanosystem.

Acknowledgements

The authors acknowledge the facilities and the scientific and technical assistance of the Australian Microscopy & Microanalysis Research Facility at the Australian Centre for Microscopy & Microanalysis at the University of Sydney. The authors gratefully acknowledge the support from the Australian Research Council for funding support (DP130104231)， the National Natural Science Foundation of China (Grant Nos. 51271148 and 50971100), the Research Fund of State Key Laboratory of Solidification Processing in China (Grant No.30-TP-2009), the Aeronautic Science Foundation Program of China (Grant No. 2012ZF53073), the Doctoral Fund of Ministry of Education of China (Grant No. 20136102110013), the Doctorate Foundation of Northwestern Polytechnical University (No.CX201104) and the Ministry of Education Fund for Doctoral Students Newcomer Awards of China.

Notes and references

[a] School of Chemical and Biomolecular Engineering, The University of Sydney, NSW 2006, Australia.

[b] The State Key Laboratory of Solidification Processing, Northwestern Polytechnical University, Xi'an 710072, China.

[c] Australian Centre for Microscopy & Microanalysis, The University of Sydney, NSW 2006, Australia.

[d] School of Materials Science and Engineering, The University of New South Wales, NSW 2052, Australia.

†Corresponding Authors: zongwen.liu@sydney.edu.au; fuyichen@nwpu.edu.cn

Electronic Supplementary Information (ESI) available: [The detailed calculated processing can be found in supplementary information]. See DOI: 10.1039/b000000x/

1 W. Wang, H. Lin, J. Li and N. Wang, *Journal of the American Ceramic Society*, 2008, **91**, 628-631.

2 G. F. Ortiz, I. Hanzu, P. Lavela, J. L. Tirado, P. Knauth and T. Djenizian, *Journal of Materials Chemistry*, 2010, **20**, 4041-4046.

3 Y. Ren, Z. Liu, F. Pourpoint, A. R. Armstrong, C. P. Grey and P. G. Bruce, *Angewandte Chemie*, 2012, **124**, 2206-2209.

4 T. Kawahara, Y. Konishi, H. Tada, N. Tohge, J. Nishii and S. Ito, *Angewandte Chemie*, 2002, **114**, 2935-2937.

5 C. Wang, X. Zhang and Y. Liu, *Nanoscale*, 2014, **6**, 5329-5337.

6 D. Yang, H. Liu, Z. Zheng, Y. Yuan, J. Zhao, E. R. Waclawik, X. Ke and H. Zhu, *Journal of the American Chemical Society*, 2009, **131**, 17885-17893.

7 R. L. Penn and J. F. Banfield, *Am. Mineral*, 1999, **84**, 871-876.

8 M. A. Henderson, *Surface Science Reports*, 2011, **66**, 185-297.

9 D. C. Hurum, A. G. Agrios, K. A. Gray, T. Rajh and M. C. Thurnauer, *The Journal of Physical Chemistry B*, 2003, **107**, 4545-4549.

10 D. O. Scanlon, C. W. Dunnill, J. Buckeridge, S. A. Shevlin, A. J. Logsdail, S. M. Woodley, C. R. A. Catlow, M. J. Powell, R. G. Palgrave and I. P. Parkin, *Nature materials*, 2013, **12**, 798-801.

11 P. I. Gouma and M. J. Mills, *Journal of the American Ceramic Society*, 2001, **84**, 619-622.

12 G. H. Lee and J. Zuo, *Journal of materials science*, 2011, **46**, 1780-1788.

13 H.-H. Lo, N. O. Gopal, S.-C. Sheu and S.-C. Ke, *The Journal of Physical Chemistry C*, 2014, **118**, 2877-2884.

14 C. Wang, X. Zhang, Y. Zhang, Y. Jia, J. Yang, P. Sun and Y. Liu, *The Journal of Physical Chemistry C*, 2011, **115**, 22276-22285.

15 W. Zhou, L. Gai, P. Hu, J. Cui, X. Liu, D. Wang, G. Li, H. Jiang, D. Liu and H. Liu, *CrystEngComm*, 2011, **13**, 6643-6649.

16 Z. Zheng, H. Liu, J. Ye, J. Zhao, E. R. Waclawik and H. Zhu, *Journal of Molecular Catalysis A: Chemical*, 2010, **316**, 75-82.

17 B. Liu, A. Khare and E. S. Aydil, *ACS applied materials & interfaces*, 2011, **3**, 4444-4450.

18 J. Zhang, Q. Xu, Z. Feng, M. Li and C. Li, *Angewandte Chemie International Edition*, 2008, **47**, 1766-1769.

19 L. Brohan, A. Verbaere, M. Tournoux and G. Demazeau, *Materials Research Bulletin*, 1982, **17**, 355-361.

20 J. F. Banfield, D. R. Veblen and D. J. Smith, *American Mineralogist*, 1991, **76**, 343-353.

21 H. Liu, Z. Zheng, D. Yang, X. Ke, E. Jaatinen, J.-C. Zhao and H. Y. Zhu, *ACS nano*, 2010, **4**, 6219-6227.

22 H. Y. Zhu, Y. Lan, X. Gao, S. P. Ringer, Z. Zheng, D. Y. Song and J. Zhao, *Journal of the American Chemical Society*, 2005, **127**, 6730-6736.

23 H. Liu, E. R. Waclawik and C. Luo, *Journal of Applied Crystallography*, 2010, **43**, 448-454.

24 H. Liu, J. Liu, L. Ouyang and C. Luo, *Journal of Applied Crystallography*, 2012, **45**, 224-233.

25 H. Liu and J. Liu, *Journal of Applied Crystallography*, 2011, **45**, 130-134.

26 T. Hahn, U. Shmueli, A. A. J. C. Wilson and E. Prince, *International tables for crystallography*, D. Reidel Publishing Company, 2005.

27 Y. Lei, J. Sun, H. Liu, X. Cheng, F. Chen and Z. Liu, *Chemistry-A European Journal*, 2014, **20**, 11313-11317.

28 J. Sun, L. Fu, H. Liu, Y. Li, S. Ringer and Z. Liu, *Journal of Alloys and Compounds*, 2014, **601**, 298-306.

29 C. Luo and U. Dahmen, *Acta materialia*, 1998, **46**, 2063-2081.

30 P. G. Embrey, *American Mineralogist*, 1986, **71**, 540-546.

31 T. P. Feist and P. K. Davies, *Journal of Solid State Chemistry*, 1992, **101**, 275-295.

32 S.-D. Mo and W. Ching, *Physical Review B*, 1995, **51**, 13023.

33 C. J. Först, C. R. Ashman, K. Schwarz and P. E. Blöchl, *Nature*, 2004, **427**, 53-56.

34 W. Li, C. Liu, Y. Zhou, Y. Bai, X. Feng, Z. Yang, L. Lu, X. Lu and K.-Y. Chan, *The Journal of Physical Chemistry C*, 2008, **112**, 20539-20545.

35 J. Mannhart and D. Schlom, *Science*, 2010, **327**, 1607-1611.